In situ stress evolution during and after sputter deposition of Al thin films

2009 J. Phys.: Condens. Matter 21 225008

(http://iopscience.iop.org/0953-8984/21/22/225008)

J. Phys.: Condens. Matter **21** (2009) 225008 (8pp) doi:10.1088/0953-8984/21/22/225008

In situ stress evolution during and after sputter deposition of Al thin films

M Pletea[1,4], R Koch[2], H Wendrock[3], R Kaltofen[1] and O G Schmidt[1]

[1] Institute for Integrative Nanosciences, IFW-Dresden, Helmholtzstraße 20, D-01069 Dresden, Germany
[2] Institute of Semiconductor and Solid State Physics, Johannes Kepler University, Altenbergerstraße 69, A-4040 Linz, Austria
[3] Institute for Complex Materials, IFW-Dresden, Helmholtzstraße 20, D-01069 Dresden, Germany

E-mail: T.M.Pletea@ifw-dresden.de

Received 10 December 2008, in final form 8 April 2009
Published 11 May 2009
Online at stacks.iop.org/JPhysCM/21/225008

Abstract
The stress, growth, and morphology evolution of Al thin films up to 300 nm thick, sputter deposited at a constant rate of 0.04 nm s^{-1} onto thermally oxidized Si(100) substrates have been investigated for various sputter pressures in the range from 0.05 to 6 Pa. The stress evolution has been studied during and after the film deposition by means of *in situ* substrate curvature measurements using an optical two-beam deflection method. In order to obtain insight into the mechanisms of stress generation and relaxation, the microstructure of the films was investigated by scanning electron microscopy, focused-ion-beam microscopy, and atomic force microscopy. The stress evolution during the early stage of deposition of films is consistent with the Volmer–Weber growth mode known for metals with high adatom mobility. For thicker films, the compressive stress increases in the sputter pressure range of 0.05–0.5 Pa, whereas at even higher sputter pressures a transition from compressive to tensile stress takes place. This transition is correlated with a change from a relatively dense to a more porous microstructure characterized by decreasing mass density and increasing electrical resistivity with increasing sputter pressure. The dependence of the stress and microstructure on the sputter pressure can be consistently understood through a combination of the stress mechanisms for vapor and sputter deposited films proposed in the literature.

1. Introduction

Thin films of aluminum and its alloys are employed as interconnects in deep submicron ultra-large scale integration (ULSI) as well as in interdigital transducers of surface acoustic waves microdevices [1–6]. Frequently, large intrinsic stress develops during film deposition independently of the growth method used (sputtering, evaporation, pulsed laser deposition, electrochemical deposition, chemical vapor deposition, etc). High intrinsic stress favors the formation of defects (e.g., voids and hillocks) and accordingly is one of the most dominant failure mechanism limiting reliability and lifetime of integrated circuits [7, 8]. On the other hand, pronounced stress gradients can efficiently shape thin solid films into three-dimensional tubular structures once the layers are released from their substrate [9, 10]. Knowledge and control of the stress evolving during and after deposition of Al films is therefore essential for understanding their physical properties and improving the performance of their applications.

While the failure mechanisms determining the performance of the integrated circuits based on Al thin films have been extensively studied [11–15], the stress data of evaporated [16, 17] and sputtered [18–20] Al films are scarce in the literature. *In situ* stress measurements during and after evaporation of Al films at room temperature (RT) [16, 17] have confirmed that Al films can be included in the group of the low-melting point metals (i.e., high adatom mobility such as Cu, Ag, Au) based on their stress development. The stress alternates from initially compressive to tensile and then back to compressive during RT evaporation of Al films, and can be understood in terms of the Volmer–Weber (VW) growth

[4] Author to whom any correspondence should be addressed.

mode [16, 21]. When Al films are sputtered, the residual stress changes from compressive to tensile with increasing sputter pressure [20]. Furthermore, due to the high chemical reactivity of Al, reactive components of the residual gas were found to have a significant effect on the growth mechanisms and related stress evolution during evaporation [16, 21]. Additionally, a thin passive layer of aluminum oxide quickly forms on the aluminum surface upon exposure to atmospheric oxygen after deposition.

In this paper, we report the results of *in situ* stress measurements during and after sputtering of Al thin films with different thicknesses and deposited at various sputtering pressures between 0.05 and 6 Pa. In order to identify possible sources of stress, microstructure investigations were performed by focused-ion-beam (FIB) microscopy, scanning electron microscopy (SEM), and atomic force microscopy (AFM). In addition, the stress behavior and microstructure of very thin layers are investigated. The stress development is compared with that of Cu films [22, 23] and discussed in terms of the models described in the literature.

2. Experimental procedure

Al films of different thicknesses ranging from 7 to 300 nm have been deposited by dc magnetron sputtering onto thermally oxidized Si(100) substrates (denoted by SiO_x). During deposition the substrates were kept at ground potential. The samples were prepared from an Al target (99.99% purity) with a diameter of 75 mm and a mean substrate–target distance of 175 mm. The base pressure of the sputter system was in the 10^{-6} Pa range. However an analysis of the sputter gas by quantitative mass spectrometry revealed the presence of water vapor with a level of 0.034% in Ar whereas nitrogen or oxygen could not be detected. The sputter pressure was varied in the range of 0.05–6 Pa. The film thickness was measured after deposition by a DEKTAK stylus profiler. In the sputter pressure range of 0.05–2 Pa a deposition rate of 0.04 nm s^{-1} was maintained requiring different discharge power (30–180 W) depending on the sputter pressure. For a sputter pressure of 6 Pa the discharge power necessary to reach a deposition rate of 0.04 nm s^{-1} corresponds to the upper limit of 300 W for the deposition system. Therefore, the growth time selected for the 6 Pa sample was half of that used for the other samples. In addition, the sample weight was measured before and after deposition in order to determine the mass density of the samples. The substrate temperature was continuously monitored during and after deposition by means of a thermocouple spot-welded directly to a stripe similar to that used for stress measurements. The details on the measurements of the substrate temperature are given in the previous papers [22, 24].

Stress evolution during and after sputter deposition of the films was investigated by means of *in situ* substrate curvature measurement using a laser-based optical bending-beam technique. The substrate deflection is proportional to the force per unit width, F/w, which is equal to the product between the average stress $\langle\sigma\rangle$ and the film thickness t_f. It is calculated via Stoney's [25] equation from the change in the position of the two laser beams on the detectors Δ_1 and Δ_2 by

$$\frac{F}{w} = \langle\sigma\rangle t_f = -\frac{1}{12}\frac{E_s}{1-\nu_s}\frac{t_s^2}{d_b L}(\Delta_2 - \Delta_1)\,. \qquad (1)$$

$E_s/(1-\nu_s)$ and t_s denote the biaxial modulus and thickness of the substrate, respectively ($E_s/(1-\nu_s) = 180.5$ GPa and $t_s = 375$ μm), d_b and L are the distance between the two parallel beams and the substrate–detector optical path, respectively ($d_b = 30$ mm and $L = 495$ mm).

During deposition of 300 nm-thick films the substrate temperature increases by 3–6 K depending on the Ar pressure. Since the thermal corrections amount only a few per cent of the intrinsic stress (compare [24]), in all figures the raw data of the stress measurements are plotted.

The microstructure analyses of the sputtered films were performed *ex situ* with a focused-ion-beam system 1540 XB and a FE-SEM Gemini 1530 (both Zeiss NTS) as well as a Veeco DI 3100 AFM. The SEM images were analyzed with a self-written image analysis sequence NANOKORN2 to estimate the island size (for details see [23]). The electrical resistance of the 300 nm-thick samples was measured at RT by the van der Pauw method.

In order to study the effect of sputter pressure on the evolution of stress and microstructure at the different stages of the growth of the Al films, three series of experiments were performed.

Series I . Al films were deposited at a growth rate of 0.04 nm s^{-1} and various sputtering pressures of 0.05, 0.2, 0.5, and 2 Pa with a final mean thickness of 300 nm.

Series II . Thin Al films with final mean thicknesses of 7, 12, and 20 nm were deposited at a rate of 0.04 nm s^{-1} and sputter pressure of 0.5 Pa.

Series III . Analogous to *series II*, but deposited at a sputter pressure of 2 Pa.

For the stress measurements of the thicker films of *series I* a slow mode was used; the experiments of *series II* and *III* concerning very thin films were performed by a rapid mode (for details see [22]).

3. Results

Figure 1 shows the evolution of the measured force per unit width $(F/w)_m$ during and after sputter deposition of 300 nm-thick Al films at RT and various sputter pressures. In the entire range of investigated sputter pressures a compressive stress contribution dominates beyond a thickness of about 20 nm. The largest compressive stress is observed at medium sputter pressure of 0.5 Pa. At low film thicknesses $(F/w)_m$ is tensile with a maximum between 10 and 20 nm depending on the sputter pressure. Starting from 0.05 Pa, the maximum shifts to lower thicknesses with increasing sputter pressure (compare inset of figure 1), but returns to higher thicknesses when the sputter pressure is raised to 2 Pa. Whereas at 2 Pa a distinct maximum can be discerned, the peak becomes smaller with decreasing sputter pressures. After finishing deposition at a

Table 1. The results of microstructure investigations, resistivity and mass density data of 300 nm-thick Al films (*series I*) as well as a 150 nm-thick Al film for various sputter pressures. The surface roughness is represented by the root mean square (RMS) value determined from $5 \times 10\ \mu m^2$ areas of the AFM images of figure 3. The area fractions of hillocks and 'open grain boundaries' are calculated as the ratio between the area of huge hills/'open grain boundaries' and the complete area of hills/grain boundaries obtained from SEM images.

Sputter pressure (Pa)	0.05	0.2	0.5	2	6
Grain size (nm) (SEM)	270	235	160	230	—
Area fraction of hillocks (%)	0.2	0.1	2.0	1.0	—
Area fraction of the 'open grain boundaries' (%)	0.7	1.0	0.9	1.9	—
Surface roughness (RMS) (nm)	6	7	11	9	—
Resistivity (10^{-8} Ω m) (resistivity of bulk Al at RT is 2.65×10^{-8} Ω m)	3.32	3.98	4.66	5.06	—
Mass density (10^3 kg m^{-3}) (mass density of bulk Al at RT is 2.70×10^3 kg m^{-3})	2.65	—	2.40	—	1.80

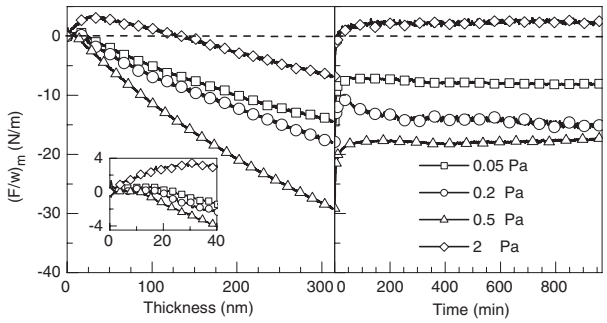

Figure 1. Evolution of the measured force per unit width $(F/w)_m$ during (left) and after (right) sputtering of 300 nm-thick Al films with a rate of 0.04 nm s^{-1} and at various Ar pressures as indicated. The inset shows the evolution of $(F/w)_m$ during the early stages of deposition.

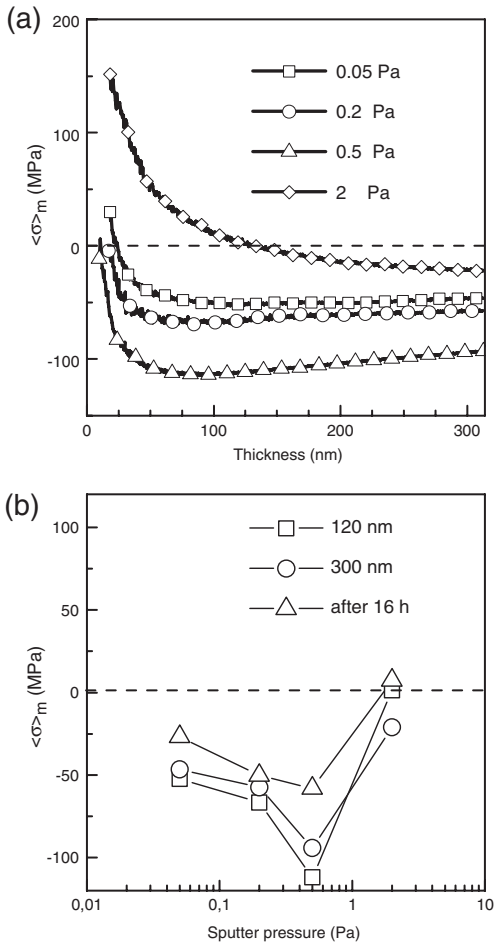

Figure 2. The evolution of the measured average stress $\langle\sigma\rangle_m$ during sputter deposition of 300 nm-thick Al films calculated by the experimental data of figure 1, for film thickness above 20 nm (a) and the measured average stress at Al thickness of 120 and 300 nm, and 16 h after deposition as a function of Ar pressure (b).

mean thickness of 300 nm, a tensile stress change is observed for approximately 30 min with the largest tensile stress rise occurring again in the 0.5 Pa film, followed by a much smaller compressive stress change that is ongoing for many hours.

The stress dependence on sputter pressure is summarized in figure 2. It shows the measured average stress $\langle\sigma\rangle_m$ calculated by equation (1) for the continuous Al films, i.e. at thicknesses above 20 nm (figure 2(a)). An inhomogeneous stress distribution over the thickness of the Al films is indicated by figure 2(a) at all sputter pressures. Figure 2(b) compares $\langle\sigma\rangle_m$ of 120 and 300 nm-thick Al films as well as the average residual stress 16 h after finishing deposition. Obviously, the stress evolving and maintained in the films depends strongly on the sputter pressure, with high compressive stress developing in the experiments at lower and medium sputter pressures (0.05, 0.2 and 0.5 Pa).

Figure 3 displays SEM and AFM images of the 300 nm-thick Al films deposited at sputter pressures of 0.05, 0.2, 0.5, and 2 Pa (*series I*). The SEM images show the typical morphology of polycrystalline films. As listed in table 1, for 300 nm-thick films the average lateral grain size decreases from 270 to 160 nm upon increasing the sputter pressure from 0.05 to 0.5 Pa; further increase to 2 Pa leads to a larger average grain size of 230 nm. AFM reveals a corrugated surface morphology with some grains (hillocks) protruding the surrounding surface at medium and higher sputter pressures (0.5 and 2 Pa). The sample deposited at medium sputter pressure of 0.5 Pa exhibits the highest surface roughness and the largest fraction of hillocks (compare table 1). We remark that the hillock concentration present after venting the sputter system is not changed in a time period of seven months (compare 0.5 Pa sample of figure 3).

Two examples of FIB images for sputter pressures of 0.2 and 2 Pa are shown in figure 4. The cross-sectional FIB images reveal that all investigated samples consist of columnar structure (e.g., figures 4(a) and (c)) with an estimated average grain size of about 200 ± 50 nm. The lateral dimensions of the grains increase with film thickness, giving the grains a conical

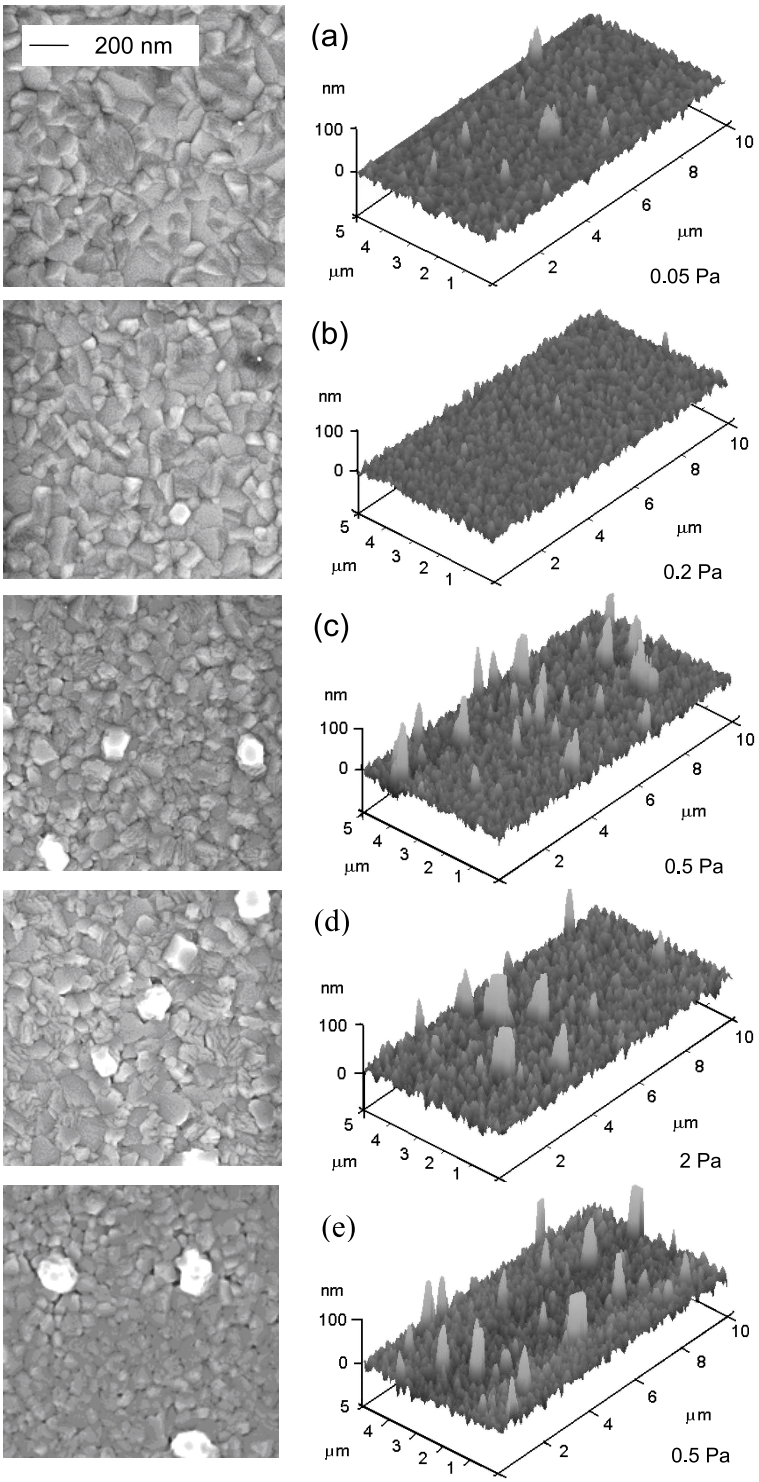

Figure 3. SEM images (left column) and AFM images (right column) of 300 nm-thick Al films sputtered with a rate of 0.04 nm s^{-1} at sputter pressures of 0.05, 0.2, 0.5, and 2 Pa ((a), (b), (c), and (d), respectively). The sample in (e) is the same as that in (c), but investigated seven months later.

shape. The top-view of FIB images reveals a similar surface topography as that obtained by SEM investigations.

The sequence of SEM images presented in figure 5 shows the surface morphology of very thin Al films with thicknesses of 7, 12, and 20 nm deposited at two different sputter pressures (0.5 and 2 Pa). For instance, the average island size of 7 nm-thick Al films decreases from 33 to 29 nm upon raising the sputter pressure from 0.5 to 2 Pa, respectively.

Both, the mass density and electrical resistivity of the Al films—also given in table 1 —depend on the sputter pressure. Whereas the mass density of the film decreases, the resistance increases with sputter pressure.

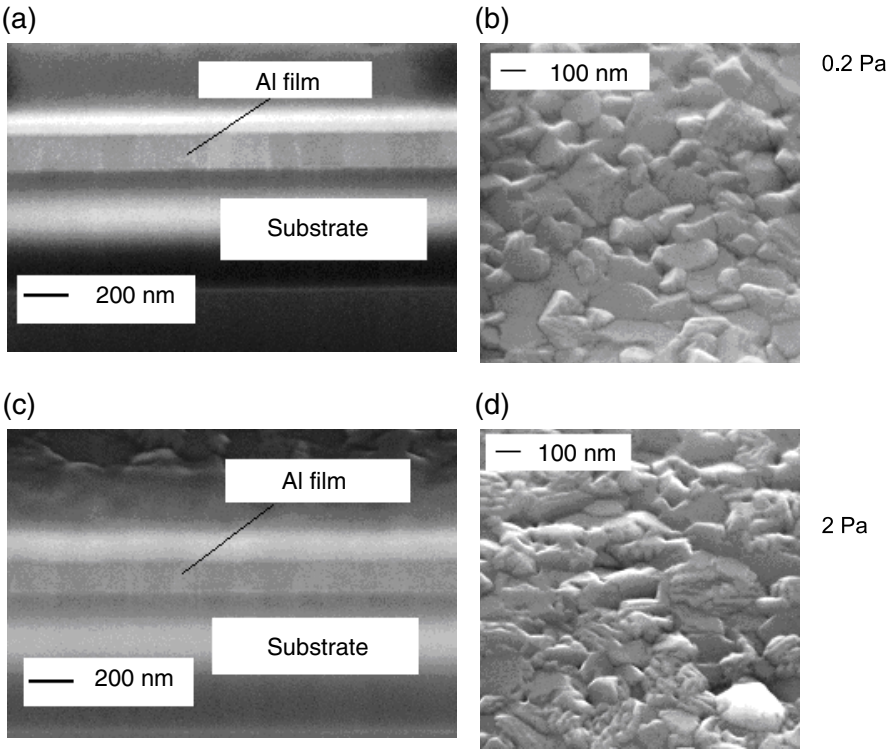

Figure 4. The cross-sectional FIB ((a) and (c)) and top-view FIB ((b) and (d)) images of 300 nm-thick Al films deposited at the indicated Ar pressures of 0.2 and 2 Pa.

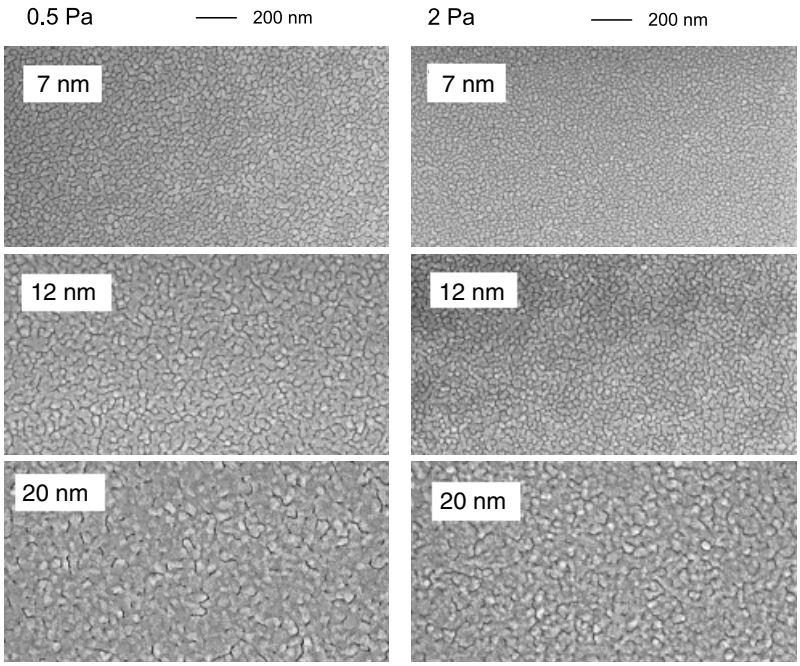

Figure 5. Sequence of SEM images of Al thin films with thicknesses of 7, 12, and 20 nm, deposited at 0.5 Pa (left column) and 2 Pa (right column).

Finally we want to remark that we had difficulties in quantitatively reproducing the F/w curves of the Al films, which is in clear contrast to the experiments with Cu published previously [22] and attributed to the higher chemical reactivity of Al compared to Cu. However, although the presented results may not be taken quantitatively, they disclose important trends due to the sputter pressure.

4. Discussion

The growth of sputtered Al films on SiO_x substrates proceeds by the VW mode, analogously to sputtered Cu [22] and Co [26] films investigated recently. This is suggested by the thickness dependence of the stress displayed in figures 1 and 2 with tensile maxima in the force curves at film thicknesses below

20 nm. It is further corroborated by the SEM investigations (figure 5) that reveal nucleation, island, percolation and channel stages until the films eventually become continuous. Grain boundary formation [27–29] in the coalescence stage as well as recrystallization of already merged grains [30, 31] give rise to a tensile stress contribution. As discussed in [21], in evaporated films the tensile maximum in $(F/w)_{\mathrm{m}}$ curves indicates the thickness at which VW films become continuous and therefore is related to island density in the discontinuous film and average island size at percolation. Surprisingly and contrary to previous results [21, 22], the height of the maximum decreases drastically with the sputter pressure and the maximum almost vanishes at a sputter pressure of 0.5 Pa (see discussion below).

Two models have been proposed in the literature for explaining the occurrence of compressive stress in continuous films: (i) in the case of evaporated VW films, a compressive strain field is generated in the island stage by capillarity effects [32–34, 17], which is propagated into the continuous film upon further growth [35]. The strain field increases with decreasing island size at percolation and decreases with film thickness due to incorporation of defects. (ii) For sputtered VW films, 'the atomic peening' effect of the energetic particles hitting the film produces the lattice distortions during film growth [36, 37]. Because plasma ions cannot arrive at a grounded substrate in dc discharge, the 'peening' effect in our experiments is predominantly determined by sputtered Al atoms and the neutralized Ar atoms back-reflected from the Al target. At low sputter pressure the back-reflected Ar atoms hit the surface of the growing film approximately with their target impact kinetic energy [37], whereas at higher sputter pressures they get thermalized, thus causing less distortion and accordingly less compressive stress.

Our experiments indicate that both mechanisms play major roles in the stress development of the sputtered Al films. Chemically more reactive materials interact with impurity molecules of the sputter gas (oxygen, water, etc) as well as of the residual gas of the vacuum system. In a previous UHV stress investigation of evaporated Al films by Abermann [16] it was found that Al interacts readily with oxygen and water already at pressures as small as 10^{-6} Pa. Increase of the partial pressure reduces the adatom mobility; as a consequence, island density increases and island size at percolation decreases, accompanied by shift of the tensile maximum to lower film thickness. Due to the higher Laplace pressure of smaller islands, the compressive stress increases considerably, e. g., from -0.02 GPa without oxygen dosage to -0.13 GPa for an oxygen partial pressure of 6×10^{-5} Pa in [16]. In our case of sputtering, the impurity concentration of the sputter gas used is 0.034%. Accordingly, the partial pressure of water vapor ranges between 1.7×10^{-5} Pa and about 2×10^{-3} Pa for Ar pressures between 0.05 and 6 Pa, respectively, which is comparable and higher, respectively, than the critical oxygen and water concentrations of Abermann's study.

The incremental compressive stress after the tensile maximum of figure 1 for sputtered films at 0.05 Pa is rather high compared to that of the evaporated films. Therefore, our experiments indicate that the effective reactivity of the impurity species may be enhanced by their higher kinetic energy leading to surface bombardment. On the one hand, due to improved sticking probability of the higher energy atoms the number of nucleation centers is increased. This leads to a higher island density and comparably smaller island size in the discontinuous films and thus larger compressive stress in the continuous films. On the other hand, reactive-atom peening may give rise to stronger damage, i.e. increased compressive stress due to peening, which may explain the strong quenching of the tensile maximum at higher sputter pressures. Consequently, the position of the tensile maximum no longer reflects the end of the discontinuous film stage.

At a sputter pressure of 2 Pa, the atom peening effect is reduced due to efficient thermalization of the bombarding species (cf [37]). Accordingly, the respective compressive stress contribution is reduced and the tensile maximum of the $(F/w)_{\mathrm{m}}$ curves recovered. Due to the simultaneous increase of the impurity pressure, the island density has further increased. This explains the decrease in island size of the discontinuous films when the sputter pressure is raised from 0.5 to 2 Pa (figure 5), a result that is opposite to that of sputtered, less reactive Cu films [22].

The results on the mass density and electrical resistivity (table 1) corroborated by SEM of a 150 nm-thick Al film, prepared at a sputter pressure of 6 Pa, indicate a more 'open' morphology (figure 6). In fact, a transition from a dense (Zone T) to a porous microstructure (Zone 1) with increasing sputter pressure is predicted by the structure-zone model of Thornton [38, 39].

Finally, we want to discuss the formation of hillocks in sputtered Al films. Our experiments indicate that hillock formation is related to the presence of compressive stress. In fact, the Al film with the largest compressive stress value (0.5 Pa) exhibits the highest hillock concentration, suggesting that hillocks are formed in order to relax compressive stress. On the basis of the experimental data we cannot unambiguously clarify at which stage the hillocks are formed. During growth there is always a decrease of the compressive stress (=decreasing slope of the $(F/w)_{\mathrm{m}}$ curves) at higher film thickness. This effective tensile stress component has been attributed to lateral grain growth in previous studies [40, 41] and may account for lateral and vertical grain growth (i.e., hillocks) as well. Moreover, a tensile stress component is observed after finishing deposition. A tensile stress change dominates for about 30 min and is followed by a small compressive stress change that continues for many hours. While short-term stress changes on the timescale of a few minutes may be due to a reversible change of the grown surface [42, 43], the main mechanism responsible for long-term stress relaxation is plastic deformation. Plastic deformation can be mediated by dislocation glide [44], the diffusion along surface and grain boundaries (Coble creep) [45], grain growth [40, 41] as well as hillock formation and growth [30, 46]. With the presented results we are not able to reliably separate the contribution of the hillock formation and growth from the other mechanisms of stress relaxation. SEM investigation of the 0.5 Pa sample seven months after preparation (see figure 3(e)) does not show a further increase

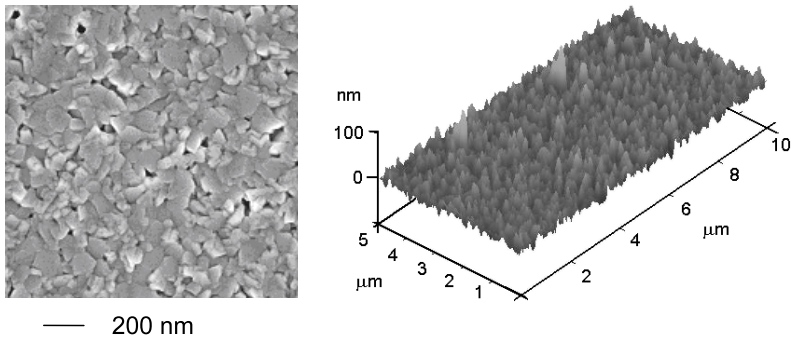

Figure 6. SEM image (left) and AFM image (right) of a 150 nm-thick Al film sputtered at sputter pressure of 6 Pa, with a rate of 0.04 nm s^{-1}.

of the hillock concentration. Therefore, the small compressive stress change ongoing for many hours is probably due to a reaction of the surface layer of the films with adsorbing molecules from the residual gas.

5. Conclusions

We have investigated stress evolution during and after sputter deposition of Al thin films with thicknesses up to 300 nm onto SiO_x substrates under various sputter pressures (figure 1). The stress evolution during early stage of deposition of Al films is related to the VW growth mode of high-mobility metals and is similar to that of sputtered Cu films concerning nuclei density, island size, and island growth. The SEM investigations (figure 5) confirm that the growth of the Al films occurs according to the VW mechanism with a discontinuous morphology at a thickness below 20 nm.

For thicker films, the compressive stress increases in the sputter pressure range of 0.05–0.5 Pa, whereas at even higher sputter pressures a transition from compressive to tensile stress takes place (figure 2). This transition is correlated with the evolution from a relatively dense to a porous microstructure, accompanied by decreasing mass density and increasing electrical resistivity. The observed stress evolution can be understood and consistently described by a combination of the stress mechanisms for vapor and sputter deposited films proposed in the literature. The stress and microstructure changes at different sputter pressures originate in the varying energy of the particles bombarding the growing Al films. To summarize, our study demonstrates that the sputter pressure affects the concentration of reactive components in the vacuum chamber and therefore is a sensitive deposition parameter for controlling growth, morphology, and stress evolution of sputtered Al films.

Acknowledgments

The authors would like to thank W Brückner for critical reading of the manuscript and for useful suggestions, B Eichler for AFM investigations, A Weckbrodt for resistivity measurements, and I Fiering and C Krien for technical assistance.

References

[1] Kimura N, Nakano M, Nakazawa M and Sato K 1997 *Japan. J. Appl. Phys.* **36** 3101
[2] Yamamoto N and Sakata S 1995 *Japan. J. Appl. Phys.* **34** 664
[3] Kimura N, Nakano M and Sato K 1998 *Japan. J. Appl. Phys.* **37** 1017
[4] Murarka S P 1997 *Mater. Sci. Eng.* R **19** 87
[5] Wang Y and Alford T L 1999 *Appl. Phys. Lett.* **74** 52
[6] Aswal D K, Muthe K P, Joshi N, Debnath A K, Gupta S K and Yakhmi J V 2003 *J. Cryst. Growth* **256** 201
[7] Murarka S P 1993 *Metallization—Theory and Practice for VLSI and ULSI* (Massachusetts: Butterworth–Heinemann) pp 83 and 84
[8] Menzel S, Schmidt H, Weihnacht M and Wetzig K 2002 *Stress-Induced Phenomena in Metallization* (New York: AIP) p 133
[9] Schmidt O G and Eberl K 2001 *Nature* **410** 168
[10] Songmuang R, Deneke Ch and Schmidt O G 2006 *Appl. Phys. Lett.* **89** 223109
[11] Eberl C, Spolenak R, Arzt E, Kubat F, Leidl A, Ruile W and Kraft O 2006 *Mater. Sci. Eng.* A **421** 68
[12] Hwang S J, Lee Y D, Park Y B, Lee J H, Jeong C O and Joo Y C 2006 *Scr. Mater.* **54** 1841
[13] Joshi N, Debnath A K, Aswal D K, Muthe K P, Kumar M S, Gupta S K and Yakhmi J V 2005 *Vacuum* **79** 178
[14] Zhang W, Brongersma S H, Richard O, Brijs B, Palmans R, Froyen L and Maex K 2004 *Microelectron. Eng.* **76** 146
[15] Buerke A, Wendrock H and Wetzig K 2000 *Cryst. Res. Technol.* **35** 721
[16] Abermann R 1990 *Thin Solid Films* **186** 233
[17] Floro J A, Hearne S J, Hunter J A, Kotula P, Chason E, Seel S C and Thomson C V 2001 *J. Appl. Phys.* **89** 4886
[18] Thornton J A and Hoffman D W 1989 *Thin Solid Films* **171** 5
[19] Chinmulgund M, Inturi R B and Barnard J A 1995 *Thin Solid Films* **270** 260
[20] Kim S P, Choi H M and Choi S K 1998 *Thin Solid Films* **322** 298
[21] Koch R 1994 *J. Phys.: Condens. Matter* **6** 9519
[22] Pletea M, Brückner W, Wendrock H and Kaltofen R 2005 *J. Appl. Phys.* **97** 054908
[23] Pletea M, Brückner W, Wendrock H, Thomas J, Kaltofen R and Koch R 2007 *J. Appl. Phys.* **101** 073511
[24] Pletea M, Wendrock H, Kaltofen R, Schmidt O G and Koch R 2008 *J. Phys.: Condens. Matter* **20** 255215
[25] Stoney G G 1909 *Proc. R. Soc.* A **82** 172
[26] Pletea M, Brückner W, Wendrock H, Kaltofen R and Koch R 2006 *J. Appl. Phys.* **99** 033509
[27] Hoffman R W 1966 *Phys. Thin Films* **3** 211
[28] Nix W D and Clemens B M 1999 *J. Mater. Res.* **14** 3467
[29] Freund L B and Chason E 2001 *J. Appl. Phys.* **89** 4866
[30] Chaudhari P 1974 *J. Appl. Phys.* **45** 4339

[31] Klokholm E and Berry B S 1968 *J. Electrochem. Soc.* **115** 823
[32] Finegan J D and Hoffman R W 1961 *AEC Technical Report 18* (Cleveland, OH: Case Institute of Technology)
[33] Abermann R, Kramer R and Mäser J 1978 *Thin Solid Films* **52** 215
[34] Cammarata R C, Trimble T M and Srolovitz D J 2000 *J. Mater. Res.* **15** 2468
[35] Abermann R, Koch R and Kramer R 1979 *Thin Solid Films* **58** 365
[36] d'Heurle F M 1970 *Metall. Trans.* **1** 725
[37] Windischmann H J 1991 *J. Vac. Sci. Technol.* A **9** 2431
[38] Thornton J A 1978 *Thin Solid Films* **54** 23
[39] Hoffman D W and Thornton J A 1980 *J. Vac. Sci. Technol.* **17** 380
[40] Koch R and Abermann R 1986 *Thin Solid Films* **140** 217
[41] Koch R, Dongzhi Hu and Das A K 2005 *Phys. Rev. Lett.* **94** 146101
[42] Spaepen F 2000 *Acta Mater.* **48** 31
[43] Chason E, Sheldon B W, Freund L B, Floro J A and Hearne S J 2002 *Phys. Rev. Lett.* **88** 156103
[44] Kraft O, Freund L B, Philips R and Arzt E 2002 *MRS Bull.* **27** 30
[45] Josell D, Weihs T P and Gao H 2002 *MRS Bull.* **27** 39
[46] Kim D K, Heiland B, Nix W D, Arzt E, Deal M D and Plummer J D 2000 *Thin Solid Films* **371** 278